

SP²T: Sparse Proxy Attention for Dual-stream Point Transformer

Jiaxu Wan^{1,*} Hong Zhang^{1,*} Ziqi He^{2,*} Qishu Wang² Ding Yuan¹ Yifan Yang^{2,†}

¹School of Aerospace, BUAA ²School of Artificial Intelligence, BUAA
<https://github.com/TerenceWalle/Sparse-Proxy-Point-Transformer>

Abstract

In 3D understanding, point transformers have yielded significant advances in broadening the receptive field. However, further enhancement of the receptive field is hindered by the constraints of grouping attention. The proxy-based model, as a hot topic in image and language feature extraction, uses global or local proxies to expand the model’s receptive field. But global proxy-based methods fail to precisely determine proxy positions and are not suited for tasks like segmentation and detection in the point cloud, and exist local proxy-based methods for image face difficulties in global-local balance, proxy sampling in various point clouds, and parallel cross-attention computation for sparse association. In this paper, we present SP²T, a local proxy-based dual stream point transformer, which promotes global receptive field while maintaining a balance between local and global information. To tackle robust 3D proxy sampling, we propose a spatial-wise proxy sampling with vertex-based point proxy associations, ensuring robust point-cloud sampling in many scales of point cloud. To resolve economical association computation, we introduce sparse proxy attention combined with table-based relative bias, which enables low-cost and precise interactions between proxy and point features. Comprehensive experiments across multiple datasets reveal that our model achieves SOTA performance in downstream tasks. The code has been released in [this url](#).

1. Introduction

The point transformer [28, 43, 44, 50] has recently emerged as a key research area in 3D perception [42] and other field [48], mainly using group attention [24, 25] to extract features. Although various point-transformer methods [43, 44] have recently advanced in expanding receptive fields, they remain constrained by the immense scale of point-cloud data. For example, the receptive field of the Point Transformer has expanded from 16 points in PTv2 [43] to 1024 points in PTv3 [44]. However, the total number of point clouds can range from 10,000 to 100,000 [1, 10], as shown in Fig. 1. Due to the constraints of group attention,

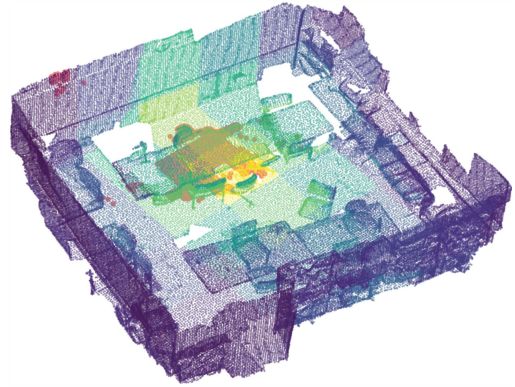


Figure 1. Receptive field comparison between PTv3 (Light Red) and ours (Overall Color).

further enlarging the receptive field in point transformer could be counterproductive. Thus, the receptive field must be broadened through alternative approaches.

For the extraction of language and image features, the proxy-based methods [11, 14, 16–18, 41] have emerged as a focus area, expanding the receptive field of neural networks while demanding less computation. These methods are generally divided into global proxy-based methods [11, 17, 18, 41] and local proxy-based methods [14, 16, 22]. Global proxy-based methods utilize proxies to exchange global information, thereby expanding the model’s receptive field. However, the methods do not accurately account for the exact positioning of the proxies and are less suited to tasks focused on local details such as segmentation and detection. Conversely, local proxy-based methods utilize the proxy sampling method to determine the proxy’s position and apply the association to depict the relationship between data and proxy, which expand the receptive field while ensure feature localization. However, the sampling and associations method for images [14, 16] proves to be challenging to implement for point clouds that exhibit diverse scales and size proportions. Moreover, when dealing with sparse point clouds, effectively parallelizing the association process based on cross-attention between proxies and points poses challenges in terms of time complexity and memory usage.

Furthermore, networks that employ proxy methods must

*Co-first author

†Corresponding author

strike a balance between global and local information. In tasks like segmentation or detection, both global and local information is of equal significance. Global features with contextual information, on the one hand, improve classification results. Conversely, the feature of the local point cloud are crucial for refining segmentation and detection bounding boxes. Drawing inspiration from MobileFormer [5], we propose that a dual-stream Transformer architecture aids in harmonizing local and global information extraction.

To address the aforementioned issues, a local proxy-based dual-stream transformer, named SP²T is introduced for point cloud understanding. Our approach involves a dual-stream Point Transformer to address the challenge of integrating local details and global information in point clouds. In SP²T, both the proxy and the point cloud are fed into the network simultaneously, allowing the balance extraction of global and local information.

Secondly, concerning proxy sampling in point clouds, we introduce a spatial-wise method employing a binary selection approach to determine the optimal proxy distribution. Subsequently, we propose a vertex-based point-proxy association method that speeds up the establishment of point-proxy associations by examining coordinate relationships through spatial-based proxy sampling.

Thirdly, to address the difficulty of efficiently computing cross-attention between the sparsely connected proxy and point, we present the sparse proxy attention (SPA). Specifically, SPA has changed from using the matrix-based attention method to using association lists, and it uses Map-Reduce [8] for parallel speed-up. Furthermore, a Table-Based Relative Bias is introduced to improve spatial awareness of SPA.

In general, the contributions of this paper include the following parts: (1) We introduce SP²T, a local proxy-based dual-stream point transformer, which effectively facilitates global receptive field while preserving a balance between global and local. (2) For the proxy sampling and association method in the sparse point cloud, a spatial-wise proxy sampling method with a vertex-based association is introduced, which ensures efficient and reliable sampling of the proxies and calculation of the association in the point cloud. (3) To address the issue of efficiently transferring information between points and proxies, Sparse Proxy Attention is introduced along with table-based relative bias. (4) Extensive experiments conducted on the many datasets [1, 3, 10] demonstrate that our model achieves state-of-the-art (SOTA) results in many downstream tasks.

2. Related Works

3D Point Cloud Understanding. Currently, methods oriented towards 3D Point Cloud Understanding can be divided into three main categories: 2D projection-based [4, 21, 23, 36], voxel-based [6, 12, 15, 26, 34, 39, 47, 51], and point cloud-based methods [29–31, 43, 44, 49, 50]. Initially, the

2D projection method utilizes the project to derive features from the point cloud using a 2D-backbone, and the voxel-based approach converts the point cloud into a structured voxel grid, which speeds up convolution or attention computations. Moreover, the point-cloud-based method processes the point-cloud directly using pooling-based or transformer architectures. SP²T is classified as a point-cloud-based network, which employs proxies to significantly expand the receptive field of the point-cloud network, thereby enhancing the model’s proficiency in understanding 3D point clouds.

Proxy-based Methods. Recently, proxy-based methods for feature extraction in both imagery and linguistics have gained considerable attention. These methods are categorized mainly into global proxy-based approaches [11, 17, 18, 41] and local proxy-based approaches [14, 16, 22]. Initially, global proxy-based techniques employ proxies to gather general information, enhancing the model’s receptive field. However, global proxies lack explicit modeling of proxy location and are not friendly to local-relevant tasks such as segmentation and detection. Secondly, local proxy-based methods focus solely on aggregating features around the proxy and incorporating information exchange between agents, thereby achieving the global receptive field. For the local proxy-based method, the sampling method and association strategy of the proxy are very important, which determine the spatial location of the proxy and the extraction range of the image. However, the sampling and association of the local proxy for point cloud data still require further investigation. SP²T employs a local proxy-based framework and examines the sampling and association method for point clouds, utilizing sparse proxy attention to expedite the computation of proxy-point interactions.

3. Method

3.1. Overall Architecture

SP²T. As illustrated in Fig. 2, SP²T is a dual-stream encoder-decoder network specifically designed for point-cloud data. Formally, the input points $P_{point} \in \mathbb{R}^{N \times 3}$ are processed through the point embedding module and the proxy initialization module to derive the feature of the point $F_{point} \in \mathbb{R}^{N \times C}$ and the proxy $F_{proxy} \in \mathbb{R}^{M \times C}$ and the position of the proxy $P_{proxy} \in \mathbb{R}^{M \times 3}$, where N and M is the number of points and proxy, and C is the embed channel.

Afterward, the positions and features of both the points and proxies are fed into a multi-stage encoder-decoder network. Each SP²TLayer is made up of several SP²TBlock for the exaction of features and ends with a downsampling or upsampling module for the point cloud and proxy to facilitate the encoding and decoding processes. Finally, the features produced by the last layer of the decoder are utilized for downstream tasks. For detailed network parameters, we report them in the *support material*.

SP²TBlock. The SP²TBlock is the foundational module in

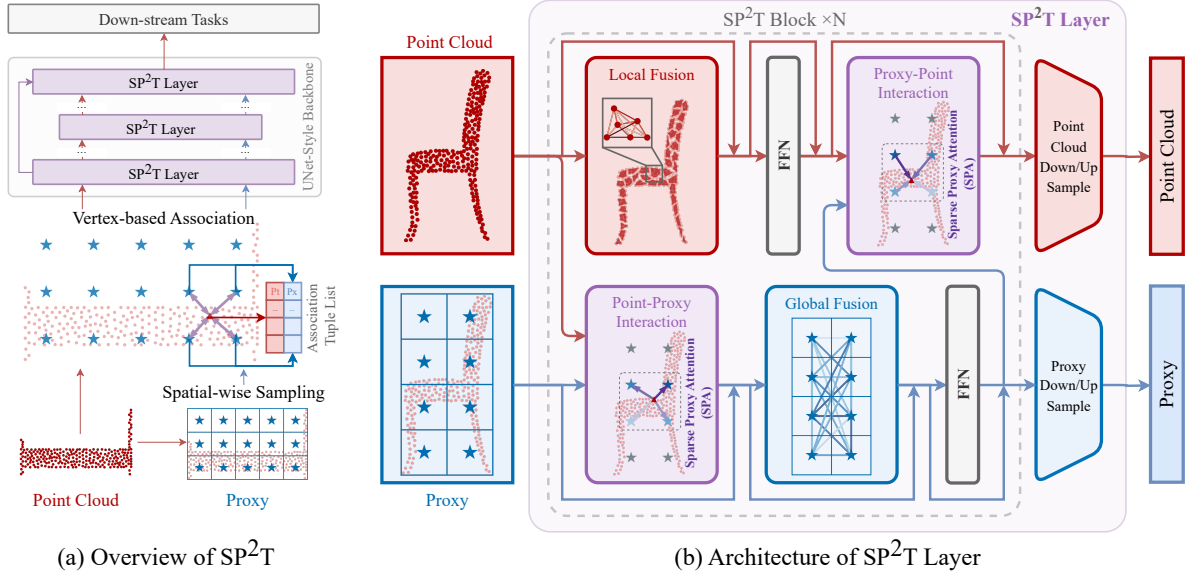


Figure 2. (a) Overview of SP²T. Followed by PTV3, our model is a U-Net Style Transformer. (b) Architecture of SP²T Layer. Every SP²T layer comprises several SP²T blocks, where both point and proxy must execute four essential operations: local fusion, point-proxy interaction, and global fusion combined with proxy-point interaction.

SP²T, enabling distinct local feature aggregation for points and global feature aggregation for proxies. SP²TBlock contains four distinct modules for feature extraction: local fusion, global fusion, point-proxy interaction, and proxy-point interaction module.

Specifically, the local fusion module is crafted to seamlessly integrate the local features of point-cloud data, while the global fusion module exceeds local receptive field limitations for a comprehensive global context understanding. Subsequently, the point-proxy and proxy-point interaction modules combine information from points and proxies using the sparse proxy attention (SPA). These modules primarily enhance the exchange of information between the point cloud and proxy, enriching point cloud features with detailed semantic context while maintaining the integrity of the proxies' local feature representation.

3.2. Proxy Sampling and Association

Problem of FPS-based Proxy Sampling. FPS-based proxy sampling utilizes the Furthest Point Sampling algorithm [30] to select a constant number of reference points from the point cloud, as widely applied in PointNet[29] and other methods. But in our method, the FPS-based approach results in a decrease in precision. Using FPS-based sampling generates a scene-relevant proxy. The model might overfit to such proxy distribution during training, resulting in a segmentation output derived directly from the scene-relevant proxy rather than from the point feature.

Problem of Grid-based Proxy Sampling Regarding grid-based proxy sampling methods, there are two primary approaches to sampling: one maintains a constant number of

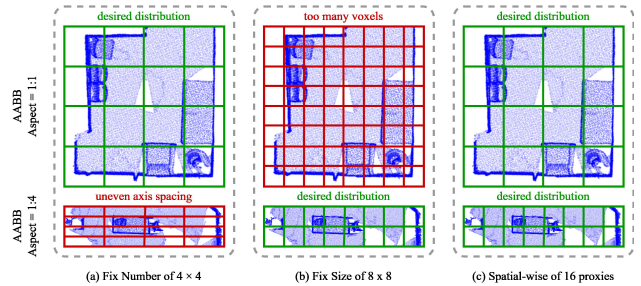


Figure 3. Comparison between different grid-based sampling methods and Spatial-wise method. (a) Fix Number of 4×4 ; (b) Fix Size of 8×8 ; (c) Spatial-wise sampling method by binary searching the square proxy spacing with a target proxy count 16.

proxies, while the other regulates a specific proxy spacing. However, each of these methods has certain challenges. Firstly, the sampling method that keeps the number of proxies constant uses a predetermined quantity $X_{voxel} \times Y_{voxel} \times Z_{voxel}$ within a uniform range. However, as illustrated in Fig. 3 (a), since the aspect ratio of the generated proxies mirrors that of the axis-aligned bounding box (AABB) of the point cloud, the proxies will appear stretched if the AABB has an extreme aspect ratio. This uneven distribution along different directions can adversely affect the uniformity of associations and feature fusion.

Secondly, the spacing-fixed sampling method separates the aspect ratio of the proxy's spacing from the point cloud by fixing the size of the proxy's spacing, enabling the uniformity of the proxies' distribution in space. However, as illustrated in Fig. 3 (b), since the AABB's range of the point cloud can fluctuate, the resultant number of proxies gener-

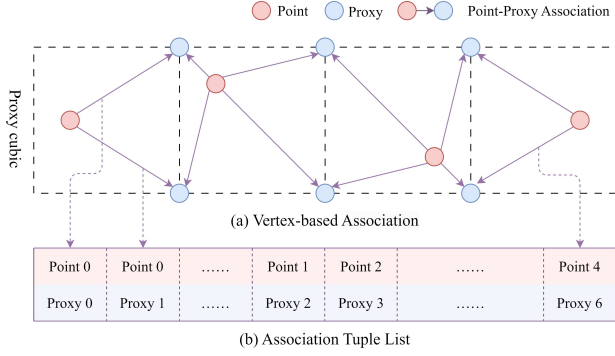


Figure 4. Overview of Vertex-based Association. In SPA, each point correlates with the proxies of the eight vertex on its respective proxy cubic.

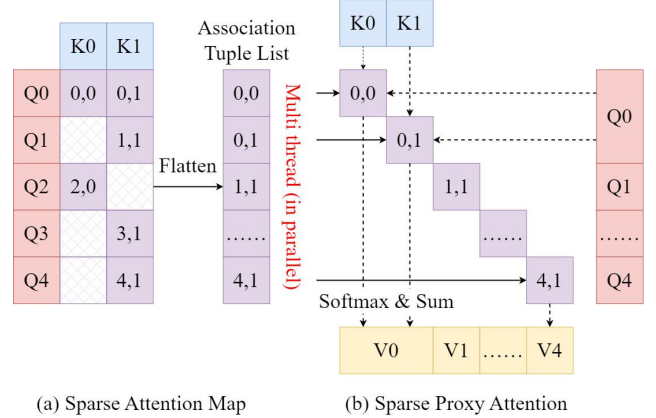
ated also varies, introducing significant uncertainty regarding the FLOPs of the model.

Spatial-wise Proxy Sampling. To address the aforementioned issues, we propose a spatial-wise proxy sampling method. Specifically, we introduced a binary search method for searching the proxy spacing. It is noted that, under an equal proxy spacing along different axis, the number of generated proxies monotonically decreases as the proxy spacing increases. Therefore, given a desired range of proxy numbers, the binary search method can be used to find an appropriate proxy spacing that brings the number of generated proxies as close as possible to the required range.

In practice, for a fixed number of proxies, our sampling method efficiently discerns the ideal proxy spacing by considering the AABB sizes of various point clouds. The method is designed to maintain the count of proxies within the bounds of N_{max} and N_{min} , using a bisection approach to determine the optimal proxy spacing L_p . If the number of proxies exceeds N_{max} , the proxy spacing L_p is reduced and the total number of proxies is recalculated. In contrast, L_p increases until the number of proxies reaches the desired range from N_{max} to N_{min} . As demonstrated in Fig. 3 (c), this method autonomously selects the best proxy spacing based on the predetermined proxy count for different point clouds depending on their AABB size. Compared to the other sampling methods in Fig. 3 (a) and (b), the spatial-wise proxy sampling method guarantees an appropriate aspect ratio for the proxy spacing and specifies a distinct number of proxies.

Vertex-based Association. A commonly adopted method for association uses the K-Nearest Neighbor (KNN) [37] method, which connects each data point with its k nearest proxies. This approach provides considerable flexibility in defining the degree of correlation between the proxies and the point cloud, thereby permitting modifications in the number of associations.

Despite this, the KNN method requires evaluating the distances between all point clouds and proxies, which adds computational complexity. In KNN using the L-Infinity Norm



(a) Sparse Attention Map

(b) Sparse Proxy Attention

Figure 5. Overview of SPA calculation. Map-reduce computing based on association tuple lists are utilized by SPA to compute sparse attention between proxy and point.

with $k = 8$, every point is linked to eight proxies positioned at the corners of a cubic proxy within the AABB coordinate sphere. As the proxy is formed through grid sampling, its structural layout can be exploited to create a more efficient association method, thereby reducing the need for intricate distance computations.

As illustrated in Fig. 4, the initial transformation involves converting the coordinates of the points to their corresponding locations within the proxy grid. Then, by computing the floor and ceiling for each coordinate, the positions of the eight nearest proxies are determined. Finally, the compilation of association tuples is achieved by aggregating all associations into one comprehensive list.

3.3. SPA for Point-Proxy Interaction

The point-proxy interaction is the fundamental concept driving SP²T. Unlike other works such as SAFDNet [46], SP²T facilitates the exchange of information between proxies and points through attention mechanisms and introduces sparse proxy attention to speed up the attention computation.

Sparse Proxy Attention (SPA). Unlike traditional attention [38], the attention between the point and the proxy is sparse and discrete due to the vertex-based connections, leading to substantial computational demands with the typical attention operator. To address this issue, we implemented sparse proxy attention to speed up information exchange between proxies and points. In practice, sparse proxy attention utilizes either the point cloud or proxy features as the query feature, while the other acts as the key and value features. Thus, it enables the aggregation of information from the point to the proxy and the feedback from the proxy back to the point.

Take the SPA that transfers features from proxy to point as an example. As shown in Fig. 5, to calculate the similarity between the proxy and the point, we denote the indices of the corresponding original points and proxy points in the i -th

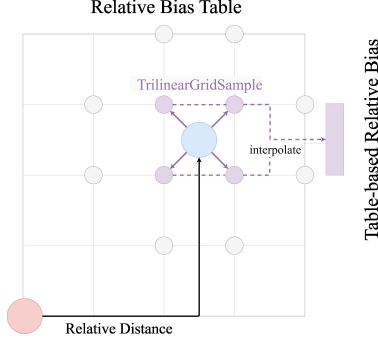


Figure 6. Overview of Table-based Relative Bias (TRB). TRB improves the spatial understanding of subsequent attention by sampling the Relative Bias Table, thus obtaining the relative bias linked to that relative distance.

association tuple as a_i^{pt}, a_i^{px} . The sparse attention module first computes the exponential similarity for the query of each association group and the key features of each head.

$$S_i^h = \exp \left(\text{dot} \left(q_{a_i^{pt}}^h, k_{a_i^{px}}^h \right) / \sqrt{d} \right) \quad (1)$$

where S_i^h is the similarity of the i -th association of the head h , $q_{a_i^{pt}}^h$ and $k_{a_i^{px}}^h$ is the query h of the head and key of a_i^{pt}, a_i^{px} . d is the dimension of the feature.

Building on this, we then employ a map-reduce algorithm to obtain the sum of exponentiated similarity over each query. Finally, a division is performed to complete the sparse softmax and obtain the weights for each value.

$$W_i^h = \frac{S_i^h}{\sum_{j, a_j^{px} = a_i^{px}} S_j^h} \quad (2)$$

where S_i^h, S_j^h is the similarity of the i -th association and the j -th association of the same proxy. W_i^h is the weight of the value after the sparse softmax.

Finally, we adopt a similar map-reduce-based method to weight the corresponding value features by the weights and association indices to obtain the output features.

$$o_i^h = \sum_{j, a_j^{px} = a_i^{px}} v_{a_j^{pt}}^h W_i^h \quad (3)$$

where $v_{a_j^{pt}}^h$ is the association value a_j^{pt} of the h th head and o_i^h is the attention output of the h th head proxy i .

Table-based Relative Bias. Inspire by the Swin Transformer [24], we found that integrating relative bias (RB) into the attention mechanism improves the network’s proficiency in capturing the connections between the proxy and the point cloud. However, the relative bias in Swin Transformer is a learning parameter synchronized with the attention map, while in SPA, the relative bias must adapt to match the dimensions of the point cloud and proxy.

To address the aforementioned issues, we introduce Table-Based Relative Bias (TRB). As shown in Fig. 6, the TRB

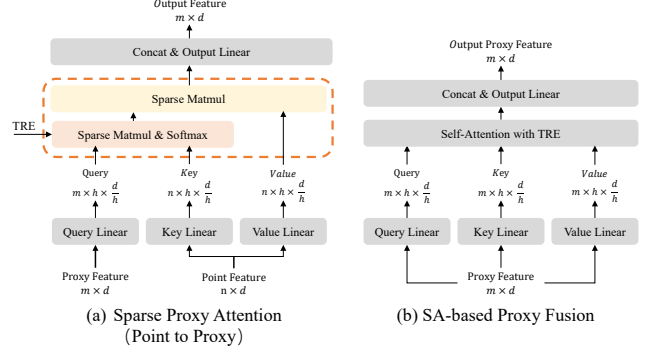


Figure 7. (a) The architecture of Sparse proxy Attention of point-proxy interaction. (b) The architecture of global fusion.

utilizes a lookup table T_{rpe} characterized by dimensions $X_{rpe}, Y_{rpe}, Z_{rpe}$. Initially, the input relative positions are converted into normalized coordinates for the lookup table by applying a scaling factor s_{rpe} . The biases are then derived at these coordinates via trilinear interpolation. Relative distances that are beyond the permissible range are clamped to valid numerical values. In terms of form, the formula for TRB is as follows.

$$TRB(x) = \text{TGS} (T_{rpe}, \text{clamp}(s_{rpe}x, -1, 1)) \quad (4)$$

where TGS is the function of the TrilinearGridSample and x is the distance between the proxy and the point. clamp is the function of the clamp number.

Finally, the similarity formula with TRB is shown as follows.

$$S_i^h = \exp \left(\text{dot} \left(q_{a_i^{pt}}^h, k_{a_i^{px}}^h \right) / \sqrt{d} \right) + \text{TRB}^h \left(p_{a_i^{pt}}^{pt} - p_{a_i^{px}}^{px} \right) \quad (5)$$

where S_i^h is the similarity of the i -th association of the head h , $q_{a_i^{pt}}^h$ and $k_{a_i^{px}}^h$ is the query of the head h and key of a_i^{pt}, a_i^{px} . d is the dimension of the feature. $p_{a_i^{pt}}^{pt}, p_{a_i^{px}}^{px}$ is the position of the point and proxy.

Furthermore, the feature dimension of the lookup table T_{rpe} is configured to match the number of heads in the sparse attention mechanism. This setup allows parallel execution of interpolation sampling and integration into similarity for each head. Furthermore, during training, the initialization of T_{rpe} used a Gaussian distribution with scaled variance, which encourages the network to initially focus on the features that are proximate.

During the implementation phase, the point and proxy positions remain unchanged within the same layer. This means that for each instance of sparse attention in this layer, the relative position input provided to the relative position encoding module remains constant. Consequently, it is possible to compute the relative bias for a layer with a single invocation. Building on this optimization, we share all relative bias values across each layer, thus reducing model complexity and computational demand. Additionally, since the proxy

Indoor Sem. Seg.	ScanNet [10]		ScanNet200 [32]		S3DIS [1]	
Methods	Val	Test	Val	Test	Area5	6-fold
PTv1 [50]	70.6	-	27.8	-	70.4	65.4
PointNeXt [31]	71.5	71.2	-	-	70.5	74.9
MinkUNet [7]	72.2	73.6	25.0	25.3	65.4	65.4
ST [20]	74.3	73.7	-	-	72.0	-
PTv2 [43]	75.4	74.2	30.2	-	71.6	73.5
PTv3 [44]	77.5	73.6 [†]	35.2	34.0 [†]	73.4	77.7
SP ² T	78.7	74.9 [†]	37.0	35.2 [†]	73.4	77.9

Table 1. Indoor semantic segmentation. [†]The result in test set of ScanNet and ScanNet200 use the PTv3’s TTA of Val Set.

Method	Metric	Area1	Area2	Area3	Area4	Area5	Area6	6-Fold
PTv2 [43]	allAcc	92.30	86.00	92.98	89.23	91.24	94.26	90.76
	mAcc	88.44	72.81	88.41	82.50	77.85	92.44	83.13
	mIoU	81.14	61.25	81.65	69.06	72.02	85.95	75.17
PTv3 [44]	allAcc	93.22	86.26	94.56	90.72	91.67	94.98	91.53
	mAcc	89.92	74.44	94.45	81.11	78.92	93.55	85.31
	mIoU	83.01	63.42	86.66	71.34	73.43	87.31	77.70
SP ² T	allAcc	92.69	87.96	93.43	90.31	91.87	94.81	91.85
	mAcc	90.21	77.74	93.67	81.85	79.24	93.48	86.03
	mIoU	83.27	64.87	86.12	71.89	73.43	87.84	77.90

Table 2. S3DIS 6-fold cross-validation.

positions are constant throughout the network, we also test sharing the relative bias amongst proxies across the entire network and across different layers.

Structure of SPA. Fig. 7 (a) illustrates the SPA structure with Point-to-Proxy. Similarly to MHSA [38], SPA incorporates four additional linear layers designed to scale down and increase the features.

3.4. Local and Global Fusion

Local Fusion The local fusion in SP²T is followed by PTv3 [44]. In particular, SP²T employs point-cloud serialization along with self-attention within PTV3 to facilitate the local fusion of point-cloud data.

Global Fusion Fig. 7 (b) illustrates the global fusion using a self-attention module with table-based relative bias. The proxy interaction module facilitates the exchange of information across all proxies, allowing each to have direct access to the global context.

4. Experiments

4.1. Result of Downstream Tasks

In this section, we will compare our model with other SOTA models in various downstream tasks. For detailed model and training settings, we report them in *supplementary material*.

Indoor Semantic Segmentation. In Tab. 1, we present the validation and test results with other methods [7, 31, 40, 43, 44, 50] on the ScanNet v2 [10] and ScanNet200 [32] benchmarks, as well as Area 5 and the 6-fold cross-validation [29]

Id. Ins. Seg.	ScanNet Val [10]			ScanNet200 Val [32]		
Baseline [19]	mAP ₂₅	mAP ₅₀	mAP	mAP ₂₅	mAP ₅₀	mAP
MinkUNet [7]	72.8	56.9	36.0	32.2	24.5	15.8
PTv2 [43]	76.3	60.0	38.3	39.6	31.9	21.4
PTv3 [44]	77.5	61.7	40.9	40.1	33.2	23.1
SP ² T	78.6	62.3	41.1	41.2	34.3	23.3

Table 3. Indoor instance segmentation.

conducted on S3DIS [1] (see Tab. 2 for detailed information). Our model demonstrated a 1.3% / 1.3% improvement in the ScanNet Val / Test set and showed an 1.8% / 1.2% increase in performance in the ScanNet200 Val / Test set compared to PTv3 [44]. In S3DIS, our performance remained consistent with PTv3 in S3DIS area5, and has a 0.2% increase in performance in S3DIS 6-fold.

As noted in the PTv3 issues on GitHub, compared to the configuration in the val-set, the PTv3 test results could have used extra test time augmentation (TTA), such as incorporating data from the validation set for training, combining results from multiple training models [20], and applying over-segmentation methods [27, 33, 45]. These augmentations may not be open source in the code of PTv3. To ensure a fair comparison, our model compares the PTv3 test results with the TTA of the val set. Furthermore, we provide more details of the test result in the supplementary material.

Indoor instance Segmentation. In Tab. 3, we provide validation outcomes for our model on the instance segmentation benchmarks of ScanNet v2 [10] and ScanNet200 [32]. Performance metrics displayed include mAP, mAP₂₅, and mAP₅₀, and are compared to various state-of-the-art (SOTA) backbones. Following PTv3 [44], we use the instance segmentation framework by utilizing PointGroup [19] in all evaluations, altering only the backbone. Compared to PTv3, we achieved enhancements of 1.1% in mAP₂₅, 0.6% in mAP₅₀, and 0.2% in mAP on ScanNet. Furthermore, in ScanNet200, there were gains of 1.1% in mAP₂₅, 0.9% in mAP₅₀, and 0.2% in mAP.

4.2. Ablation Study

Followed by PTv3, the model’s ablation studies were conducted on the ScanNet validation set, where four metrics, including mIOU, mAcc, allAcc and latency. The latency is reported using a single 4090 GPU with 1 batch size.

The number of proxy and association. Tab. 4 presents the ablation study exploring the impact of the number of proxies and associations in SP²T. Experimental results indicate that increasing the number of proxies and associations does not always result in better performance. On the one hand, an excess of proxies leads to a shortage of corresponding point clouds, thereby restricting the model’s receptive field. On the other hand, an abundance of associations generates numerous point clouds linked to the proxies, making it difficult for the proxy to accurately represent the point cloud. As a result,

Number		Method	Metrics			
Proxy	Association	Association	mIoU	mAcc	allAcc	Time/ms
Baseline (PTV3)			77.51	85.16	92.24	61
40	8	Vertex	77.74	86.39	92.05	65
80	8	Vertex	77.79	86.11	92.17	68
120	8	Vertex	77.71	86.22	92.43	71
160	8	Vertex	78.71	86.23	92.51	74
320	8	Vertex	78.08	86.15	92.31	92
512	8	Vertex	78.22	86.60	92.30	120
800	8	Vertex	77.79	85.83	92.01	221
160	4	KNN	77.99	86.61	92.22	69
160	8	KNN	78.71	86.23	92.51	83
160	12	KNN	77.90	85.77	92.19	97
160	16	KNN	78.10	86.99	92.40	158

Table 4. Ablation study about the number of proxy and association of SP²T in ScanNet. KNN utilizes the L-Infinity norm for measuring distance.

TRB	FPS	Fix Number	Fix Size	Spatial-wise
✗	77.38	77.74	OOM	78.05
✓	78.24	78.35	OOM	78.71

Table 5. Ablation study about proxy sample method and TRB in ScanNet. OOM means Out of Memory.

Share TRB	mIoU	mAcc	allAcc	Time
✗	78.03	86.17	92.36	81ms
✓	78.71	86.23	92.51	74ms

Table 6. Ablation study about parameter sharing of TRB.

the ideal number of proxies and associations is essential to produce the best results.

Proxy Sampling Method and Table-based Relative Bias. Tab. 5 provides the results of the ablation study on proxy sampling methods and Table-based Relative Bias. The experiment indicates that the spatial-wise sampling method yields the best model accuracy among various sampling methods. Additionally, TRB is adaptable to all sampling methods and can generally enhance model performance. Particularly with respect to the sampling method, the Fix Number and Fix Size-based methods struggle with point clouds at different scales, resulting in reduced accuracy and failure training. In contrast, the spatial-wise sampling approach can flexibly determine the proxy spacing thereby improving performance. Regarding the FPS-based method, the analysis is provided in the Discussion regarding the low performance of the FPS-based sampling method.

Share of Table Relative Bias. Tab. 6 shows a comparison of the accuracy of the model w/ and w/o the shared TRB. The experiment shows that the shared TRB both improves the accuracy of the model and reduces the inference time. Furthermore, Fig. 8 shows the MSE distance for TRB during point-proxy and proxy-proxy interaction in different layers. In total, TRB demonstrates stage-level similarity in

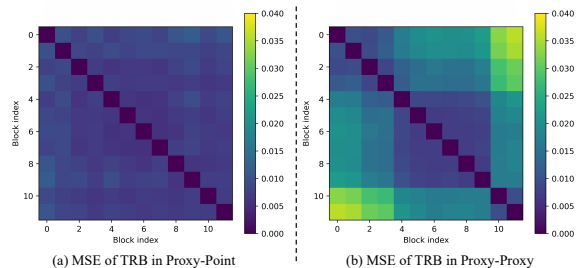


Figure 8. (a) MSE of TRB in different proxy-point interaction layer. (b) MSE of TRB in different proxy-proxy interaction layer.

Empty Proxy	mIoU	mAcc	allAcc
✗	77.80	86.61	91.97
✓	78.71	86.23	92.51

Table 7. Ablation study about empty proxies.

Efficiency	Indoor (ScanNet [10])		Outdoor (nuScenes [3])	
Methods	mIOU	Latency	mIOU	Latency
MinkUNet [7]	72.2	90ms	73.3	48ms
PTv2 [43]	75.4	191ms	80.2	146ms
PTv3 [44]	77.5	61ms	80.4	44ms
SP ² T	78.7	74ms	81.2	54ms

Table 8. Ablation study about efficiency of SP²T.

the proxy-proxy interaction, while all TRB is similar in the point-proxy interaction. Consequently, the sharing of TRB improves model accuracy and reduces inference time.

Empty Proxies. Different from image, grid sampling in point cloud unavoidably results in empty proxies, which lack any point cloud association. Tab. 7 presents a comparison of SP²T accuracy both with and without considering empty proxies during global fusion. The experimental data indicate that empty proxies actually enhance the accuracy of the model. We believe that the experiment proves that ‘nothing’ is also a very important piece of information in the point cloud. Although empty proxies lack point-cloud data, the absence itself conveys spatial structure information, thereby contributing to an understanding of overall spatial feature for point cloud.

Model efficiency. Tab. 8 illustrates the model’s efficiency, evaluated in terms of accuracy and latency, for both indoor (ScanNet) and outdoor (nuScenes) datasets using a single RTX 4090. We compared our model with PTv3, PTv2, and MinkUnet. Although our model runs slower than PTv3, our model achieves the best balance of accuracy and latency in both indoor and outdoor datasets.

4.3. Discussion and Visualization

In this section, we discuss the limitations of the FPS sampling method and illustrate the attention map of SPA. More discussion and visualization are provided in *support materials*.

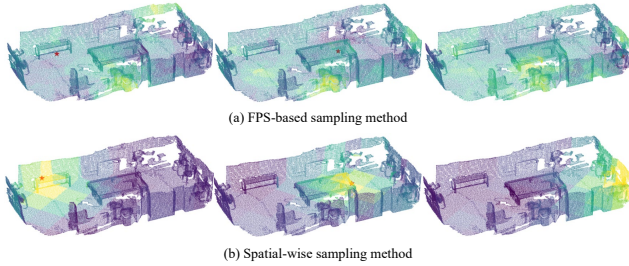


Figure 9. Visualization of the point-point attention map under FPS-based and Spatial-wise proxy sampling method. The red star represents the current point.

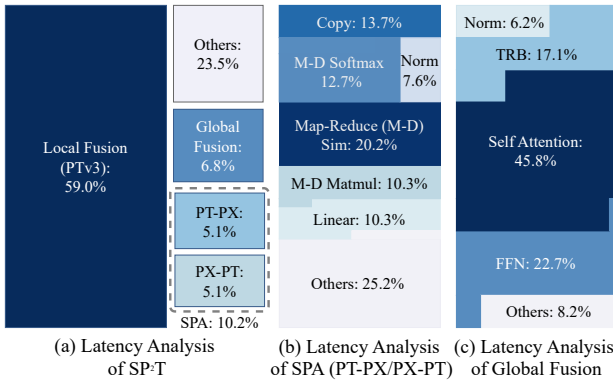


Figure 10. Visualization of the latency of SP^2T , Sparse Proxy Attention and Global Fusion. The latency of local and global fusion include the latency of FFN.

Over-fitting due to FPS-based Sampling. Within the ablation study, the experiments show that FPS-based sampling performs poorly compared to alternative sampling methods. To investigate this further, we visualized the point-proxy attention maps for both FPS-based and Spatial-wise sampling methods, as illustrated in Fig. 9. The visualization illustrates that the attention map resulting from FPS-based sampling exhibits static and repetitive patterns, with its attention not influenced by the proxy’s location. On the other hand, the attention map from spatial-wise sampling aligns with typical attention maps and takes the proxy location into account. Consequently, we contend that the sampling method based on FPS leads to significant overfitting of the model because of the scene leakage from FPS.

Visualization of Latency. Fig. 10 (a) presents the latency tree map for our model. It reveals that SPA and global fusion contribute 17% to overall latency. The latency of local and global fusion include the latency of FFN. Additionally, Fig. 10 (b) & (c) display the latency tree map of each operator in SPA and global fusion. The findings indicate that SPA with global fusion significantly improves performance without imposing substantial delay.

Visualization of SPA. Fig. 11 provides a depiction of the attention map in SPA, focusing on the interaction between the point and the proxy. Specifically, Fig. 11 (a) highlights the attention map from point to proxy, and Fig. 11 (b) showcases

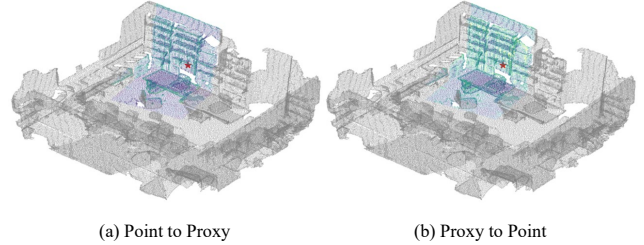


Figure 11. Visualization of Point-Proxy and Proxy-Point Attention Map of SPA. The red star represents the current proxy.

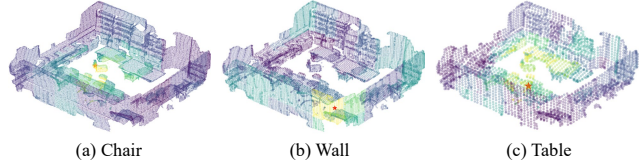


Figure 12. Visualization of Point to Point Attention Map of SPA of different objects and stages (with different downsampling rate). The red star represents the current point.

the return path from proxy to point. Examining the visualization reveals that the SPA’s semantic mining capability is evident. In this visualization, as the chosen proxy approaches the bookshelf, both the point cloud and the proxy’s focus show a stronger affinity for the bookshelf compared to the table, showcasing the SPA’s semantic representation ability.

By processing the attention maps of point-to-proxy, proxy-to-proxy, and proxy-to-point, we can derive the corresponding point-to-point attention maps in SPA. Fig. 12 illustrates the point-to-point SPA attention map at different stages (with different downsampling rates). The visualization results indicate that SPA is capable of demonstrating semantic aggregation at different stages. This includes the focused attention of a point on one chair toward other chairs in Fig. 12 (a), the focus of a point on the wall towards the entire wall in Fig. 12 (b), and the attention of a point on the table towards other tables in Fig. 12 (c).

5. Conclusion

In this paper, we introduce SP^2T , a local proxy-based dual-stream point transformer that uses sparse proxy attention to achieve global receptive field. To address the proxy sampling challenges in point clouds, we propose a spatial-wise proxy sampling method with vertex-based association, which ensures efficient and reliable proxy sampling and association calculations. Moreover, we also address the point-proxy cross-attention problem by incorporating sparse proxy attention with table-based relative bias, which enhances precise interactions between proxy and point features. Comprehensive experiments across multiple datasets show that our model achieves state-of-the-art performance in various downstream tasks. For limitations, we claim that the implementation of SPA and network parameters can be further refined. Compared to PTV3, our method uses more time and memory, and we will continue this research to address these challenges.

References

- [1] Iro Armeni, Ozan Sener, Amir R Zamir, Helen Jiang, Ioannis Brilakis, Martin Fischer, and Silvio Savarese. 3d semantic parsing of large-scale indoor spaces. In *Proceedings of the IEEE conference on computer vision and pattern recognition*, pages 1534–1543, 2016. 1, 2, 6, 12
- [2] Maxim Berman, Amal Rannen Triki, and Matthew B Blaschko. The lovász-softmax loss: A tractable surrogate for the optimization of the intersection-over-union measure in neural networks. In *Proceedings of the IEEE conference on computer vision and pattern recognition*, pages 4413–4421, 2018. 12
- [3] Holger Caesar, Varun Bankiti, Alex H Lang, Sourabh Vora, Venice Erin Liong, Qiang Xu, Anush Krishnan, Yu Pan, Giancarlo Baldan, and Oscar Beijbom. nuscenes: A multi-modal dataset for autonomous driving. In *Proceedings of the IEEE/CVF conference on computer vision and pattern recognition*, pages 11621–11631, 2020. 2, 7, 12
- [4] Xiaozhi Chen, Huimin Ma, Ji Wan, Bo Li, and Tian Xia. Multi-view 3d object detection network for autonomous driving. In *Proceedings of the IEEE conference on Computer Vision and Pattern Recognition*, pages 1907–1915, 2017. 2
- [5] Yinpeng Chen, Xiyang Dai, Dongdong Chen, Mengchen Liu, Xiaoyi Dong, Lu Yuan, and Zicheng Liu. Mobile-former: Bridging mobilenet and transformer. In *Proceedings of the IEEE/CVF conference on computer vision and pattern recognition*, pages 5270–5279, 2022. 2
- [6] Yukang Chen, Jianhui Liu, Xiangyu Zhang, Xiaojuan Qi, and Jiaya Jia. Voxelnex: Fully sparse voxelnet for 3d object detection and tracking. In *Proceedings of the IEEE/CVF Conference on Computer Vision and Pattern Recognition*, pages 21674–21683, 2023. 2
- [7] Christopher Choy, JunYoung Gwak, and Silvio Savarese. 4d spatio-temporal convnets: Minkowski convolutional neural networks. In *Proceedings of the IEEE/CVF conference on computer vision and pattern recognition*, pages 3075–3084, 2019. 6, 7, 11, 13
- [8] Cheng-Tao Chu, Sang Kim, Yi-An Lin, YuanYuan Yu, Gary Bradski, Kunle Olukotun, and Andrew Ng. Map-reduce for machine learning on multicore. *Advances in neural information processing systems*, 19, 2006. 2
- [9] Pointcept Contributors. Pointcept: A codebase for point cloud perception research. <https://github.com/Pointcept/Pointcept>, 2023. 12
- [10] Angela Dai, Angel X Chang, Manolis Savva, Maciej Halber, Thomas Funkhouser, and Matthias Nießner. Scannet: Richly-annotated 3d reconstructions of indoor scenes. In *Proceedings of the IEEE conference on computer vision and pattern recognition*, pages 5828–5839, 2017. 1, 2, 6, 7, 11, 12
- [11] Timothée Darcet, Maxime Oquab, Julien Mairal, and Piotr Bojanowski. Vision transformers need registers. *arXiv preprint arXiv:2309.16588*, 2023. 1, 2
- [12] Lue Fan, Ziqi Pang, Tianyuan Zhang, Yu-Xiong Wang, Hang Zhao, Feng Wang, Naiyan Wang, and Zhaoxiang Zhang. Embracing single stride 3d object detector with sparse transformer. In *Proceedings of the IEEE/CVF conference on computer vision and pattern recognition*, pages 8458–8468, 2022. 2
- [13] Pedro F Felzenszwalb and Daniel P Huttenlocher. Efficient graph-based image segmentation. *International journal of computer vision*, 59:167–181, 2004. 11
- [14] Dongchen Han, Tianzhu Ye, Yizeng Han, Zhuofan Xia, Siyuan Pan, Pengfei Wan, Shiji Song, and Gao Huang. Agent attention: On the integration of softmax and linear attention. *arXiv preprint arXiv:2312.08874*, 2023. 1, 2
- [15] Chenheng He, Ruihuang Li, Guowen Zhang, and Lei Zhang. Scatterformer: Efficient voxel transformer with scattered linear attention. *arXiv preprint arXiv:2401.00912*, 2024. 2
- [16] Huaibo Huang, Xiaoqiang Zhou, Jie Cao, Ran He, and Tieniu Tan. Vision transformer with super token sampling. In *Proceedings of the IEEE/CVF conference on computer vision and pattern recognition*, pages 22690–22699, 2023. 1, 2
- [17] Andrew Jaegle, Sebastian Borgeaud, Jean-Baptiste Alayrac, Carl Doersch, Catalin Ionescu, David Ding, Skanda Koppula, Daniel Zoran, Andrew Brock, Evan Shelhamer, et al. Perceiver io: A general architecture for structured inputs & outputs. *arXiv preprint arXiv:2107.14795*, 2021. 1, 2
- [18] Andrew Jaegle, Felix Gimeno, Andy Brock, Oriol Vinyals, Andrew Zisserman, and Joao Carreira. Perceiver: General perception with iterative attention. In *International conference on machine learning*, pages 4651–4664. PMLR, 2021. 1, 2
- [19] Li Jiang, Hengshuang Zhao, Shaoshuai Shi, Shu Liu, Chi-Wing Fu, and Jiaya Jia. Pointgroup: Dual-set point grouping for 3d instance segmentation. In *Proceedings of the IEEE/CVF conference on computer vision and Pattern recognition*, pages 4867–4876, 2020. 6, 13
- [20] Xin Lai, Jianhui Liu, Li Jiang, Liwei Wang, Hengshuang Zhao, Shu Liu, Xiaojuan Qi, and Jiaya Jia. Stratified transformer for 3d point cloud segmentation. In *Proceedings of the IEEE/CVF conference on computer vision and pattern recognition*, pages 8500–8509, 2022. 6, 11
- [21] Alex H Lang, Sourabh Vora, Holger Caesar, Lubing Zhou, Jiong Yang, and Oscar Beijbom. Pointpillars: Fast encoders for object detection from point clouds. In *Proceedings of the IEEE/CVF conference on computer vision and pattern recognition*, pages 12697–12705, 2019. 2
- [22] Juho Lee, Yoonho Lee, Jungtaek Kim, Adam Kosior, Seungjin Choi, and Yee Whye Teh. Set transformer: A framework for attention-based permutation-invariant neural networks. In *International conference on machine learning*, pages 3744–3753. PMLR, 2019. 1, 2
- [23] Bo Li, Tianlei Zhang, and Tian Xia. Vehicle detection from 3d lidar using fully convolutional network. *arXiv preprint arXiv:1608.07916*, 2016. 2
- [24] Ze Liu, Yutong Lin, Yue Cao, Han Hu, Yixuan Wei, Zheng Zhang, Stephen Lin, and Baining Guo. Swin transformer: Hierarchical vision transformer using shifted windows. In *Proceedings of the IEEE/CVF international conference on computer vision*, pages 10012–10022, 2021. 1, 5
- [25] Ze Liu, Han Hu, Yutong Lin, Zhuliang Yao, Zhenda Xie, Yixuan Wei, Jia Ning, Yue Cao, Zheng Zhang, Li Dong, et al. Swin transformer v2: Scaling up capacity and resolution. In

- Proceedings of the IEEE/CVF conference on computer vision and pattern recognition*, pages 12009–12019, 2022. 1
- [26] Daniel Maturana and Sebastian Scherer. Voxnet: A 3d convolutional neural network for real-time object recognition. In *2015 IEEE/RSJ international conference on intelligent robots and systems (IROS)*, pages 922–928. IEEE, 2015. 2
- [27] Alexey Nekrasov, Jonas Schult, Or Litany, Bastian Leibe, and Francis Engelmann. Mix3d: Out-of-context data augmentation for 3d scenes. In *2021 international conference on 3d vision (3dv)*, pages 116–125. IEEE, 2021. 6
- [28] Chung Hyun Park, Yoonwoo Jeong, Minsu Cho, and Jaesik Park. Fast point transformer. In *Proceedings of the IEEE/CVF conference on computer vision and pattern recognition*, pages 16949–16958, 2022. 1
- [29] Charles R Qi, Hao Su, Kaichun Mo, and Leonidas J Guibas. Pointnet: Deep learning on point sets for 3d classification and segmentation. In *Proceedings of the IEEE conference on computer vision and pattern recognition*, pages 652–660, 2017. 2, 3, 6
- [30] Charles Ruizhongtai Qi, Li Yi, Hao Su, and Leonidas J Guibas. Pointnet++: Deep hierarchical feature learning on point sets in a metric space. *Advances in neural information processing systems*, 30, 2017. 3
- [31] Guocheng Qian, Yuchen Li, Houwen Peng, Jinjie Mai, Hasan Hammoud, Mohamed Elhoseiny, and Bernard Ghanem. Pointnext: Revisiting pointnet++ with improved training and scaling strategies. *Advances in neural information processing systems*, 35:23192–23204, 2022. 2, 6
- [32] David Rozenberszki, Or Litany, and Angela Dai. Language-grounded indoor 3d semantic segmentation in the wild. In *European Conference on Computer Vision*, pages 125–141. Springer, 2022. 6, 11, 12
- [33] Jonas Schult, Francis Engelmann, Alexander Hermans, Or Litany, Siyu Tang, and Bastian Leibe. Mask3d: Mask transformer for 3d semantic instance segmentation. In *2023 IEEE International Conference on Robotics and Automation (ICRA)*, pages 8216–8223. IEEE, 2023. 6, 11
- [34] Shuran Song, Fisher Yu, Andy Zeng, Angel X Chang, Manolis Savva, and Thomas Funkhouser. Semantic scene completion from a single depth image. In *Proceedings of the IEEE conference on computer vision and pattern recognition*, pages 1746–1754, 2017. 2
- [35] Nitish Srivastava, Geoffrey Hinton, Alex Krizhevsky, Ilya Sutskever, and Ruslan Salakhutdinov. Dropout: a simple way to prevent neural networks from overfitting. *The journal of machine learning research*, 15(1):1929–1958, 2014. 13
- [36] Hang Su, Subhransu Maji, Evangelos Kalogerakis, and Erik Learned-Miller. Multi-view convolutional neural networks for 3d shape recognition. In *Proceedings of the IEEE international conference on computer vision*, pages 945–953, 2015. 2
- [37] Kashvi Taunk, Sanjukta De, Srishti Verma, and Aleena Sweapadma. A brief review of nearest neighbor algorithm for learning and classification. In *2019 international conference on intelligent computing and control systems (ICCS)*, pages 1255–1260. IEEE, 2019. 4
- [38] A Vaswani. Attention is all you need. *Advances in Neural Information Processing Systems*, 2017. 4, 6
- [39] Haiyang Wang, Chen Shi, Shaoshuai Shi, Meng Lei, Sen Wang, Di He, Bernt Schiele, and Liwei Wang. Dsvt: Dynamic sparse voxel transformer with rotated sets. In *Proceedings of the IEEE/CVF Conference on Computer Vision and Pattern Recognition*, pages 13520–13529, 2023. 2
- [40] Peng-Shuai Wang. Octformer: Octree-based transformers for 3d point clouds. *ACM Transactions on Graphics (TOG)*, 42(4):1–11, 2023. 6, 11
- [41] Sinong Wang, Belinda Z Li, Madian Khabsa, Han Fang, and Hao Ma. Linformer: Self-attention with linear complexity. *arXiv preprint arXiv:2006.04768*, 2020. 1, 2
- [42] Yue Wang, Vitor Campagnolo Guizilini, Tianyuan Zhang, Yilun Wang, Hang Zhao, and Justin Solomon. Detr3d: 3d object detection from multi-view images via 3d-to-2d queries. In *Conference on Robot Learning*, pages 180–191. PMLR, 2022. 1
- [43] Xiaoyang Wu, Yixing Lao, Li Jiang, Xihui Liu, and Hengshuang Zhao. Point transformer v2: Grouped vector attention and partition-based pooling. *Advances in Neural Information Processing Systems*, 35:33330–33342, 2022. 1, 2, 6, 7
- [44] Xiaoyang Wu, Li Jiang, Peng-Shuai Wang, Zhijian Liu, Xihui Liu, Yu Qiao, Wanli Ouyang, Tong He, and Hengshuang Zhao. Point transformer v3: Simpler faster stronger. In *Proceedings of the IEEE/CVF Conference on Computer Vision and Pattern Recognition*, pages 4840–4851, 2024. 1, 2, 6, 7, 11, 13
- [45] Yu-Qi Yang, Yu-Xiao Guo, Jian-Yu Xiong, Yang Liu, Hao Pan, Peng-Shuai Wang, Xin Tong, and Baining Guo. Swin3d: A pretrained transformer backbone for 3d indoor scene understanding. *arXiv preprint arXiv:2304.06906*, 2023. 6, 11
- [46] Gang Zhang, Junnan Chen, Guohuan Gao, Jianmin Li, Si Liu, and Xiaolin Hu. Safdnet: A simple and effective network for fully sparse 3d object detection. In *Proceedings of the IEEE/CVF Conference on Computer Vision and Pattern Recognition*, pages 14477–14486, 2024. 4
- [47] Hong Zhang, Jiaxu Wan, Ziqi He, Jianbo Song, Yifan Yang, and Ding Yuan. Sparse agent transformer for unified voxel and image feature extraction and fusion. *Information Fusion*, page 102455, 2024. 2
- [48] Hong Zhang, Jiaxu Wan, Jing Zhang, Ding Yuan, XuLiang Li, and Yifan Yang. P2track: Multi-object tracking with motion prior and feature posterior. *ACM Transactions on Multimedia Computing, Communications and Applications*, 2024. 1
- [49] Hengshuang Zhao, Li Jiang, Chi-Wing Fu, and Jiaya Jia. Pointweb: Enhancing local neighborhood features for point cloud processing. In *Proceedings of the IEEE/CVF conference on computer vision and pattern recognition*, pages 5565–5573, 2019. 2
- [50] Hengshuang Zhao, Li Jiang, Jiaya Jia, Philip HS Torr, and Vladlen Koltun. Point transformer. In *Proceedings of the IEEE/CVF international conference on computer vision*, pages 16259–16268, 2021. 1, 2, 6
- [51] Yin Zhou and Oncel Tuzel. Voxnet: End-to-end learning for point cloud based 3d object detection. In *Proceedings of the IEEE conference on computer vision and pattern recognition*, pages 4490–4499, 2018. 2

Indoor Sem. Seg.	ScanNet [10]		ScanNet200 [32]	
	Val	Test	Val	Test
Methods with same TTA				
MinkUnet [7]	72.2	73.4	25.0	25.3
OctFormer [40] [†]	74.6	70.7	31.9	31.0
Swin3D [45] [†]	76.6	71.4	-	-
PTv3 [44] [‡]	77.5	73.6	35.2	34.0
SP ² T	78.7	74.9	37.0	35.2

Table 9. Indoor instance segmentation with same TTA between Val and Test set. [†]Reproduction using code of Pointcept. [‡]Official weight and code.

Indoor Sem. Seg.	ScanNet [10]		ScanNet200 [32]	
	Val	Test	Val	Test
Methods				
MinkUnet [7]	72.2	73.4	25.0	25.3
SP ² T w/ MinkUnet	74.7(↑2.5)	-	28.3(↑3.3)	-
PTv3 [44]	77.5	73.6	35.2	34.0
SP ² T w/ PTv3	78.7(↑1.2)	74.9(↑1.3)	37.0(↑1.8)	35.2(↑1.2)

Table 10. Transfer study of local fusion.

A. Experiment and Discussion

A.1. Result Gap in Test Set

According to [33, 44, 45], there is a large test time augmentation (TTA) difference between the val and test sets of Scannet [10] and Scannet200 [32]. The additional TTA includes incorporating data from the validation set for training, combining results from multiple training models [20], and applying over-segmentation [13].

For fair comparison, we evaluated some SOTA models [7, 40, 44, 45] with an official or reproduction weights file using Val’s TTA, as shown in Fig. 9. The experimental findings indicate that, without employing additional TTA, the result in the test set for the majority models [40, 44, 45] tends to be less than those on the validation set, rather than exceeding them. And it can be found that our model archive the best result both in the val and test set of Scannet and Scannet200.

We are still working on over-segmentation and may update our model’s test results employing over-segmentation in the final version of the paper. Furthermore, we recommend that future research ensure consistency in the TTA between the validation set and the test set, or at least make the TTA on the test set openly available. In the field of 3D understanding, the focus should be on improving network design and training methodologies rather than on using more testing tricks.

A.2. Transfer Study of Local Fusion

We also use MinkUnet [7] as the local fusion module to test the portability of our design. Tab. 10 shows the performance of MinkUnet [7] and PTv3 [44] and its variants with our proposed sparse proxy attention mechanism on the Scannet [10] and Scannet200 [32] datasets. The experimental results demonstrate that our network structure is plug-and-

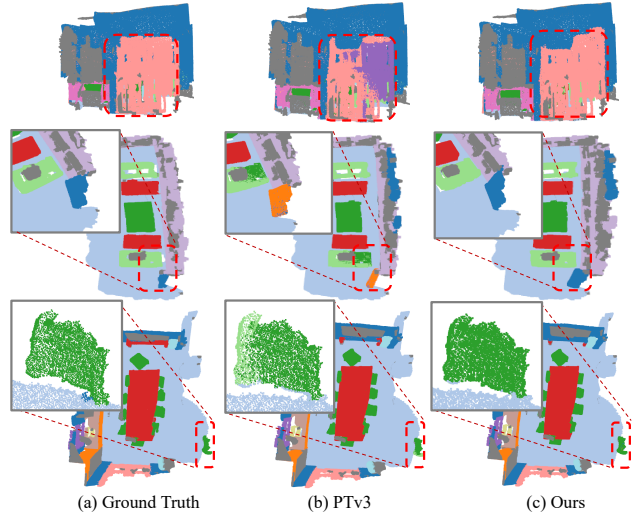


Figure 13. Result Comparison in ScanNet.

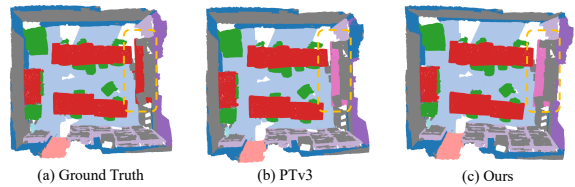


Figure 14. Failed cases in ScanNet.

play and can integrate seamlessly with various local fusion networks, thereby enhancing the receptive field and boosting the network’s performance.

A.3. Visualization

Result Comparison. Fig. 13 compares the visualization of our method and PTv3 [44] on the Scannet dataset [10]. Specifically, Fig. 13 (a) presents the ground truth, Fig. 13 (b) depicts the result from PTv3, and Fig. 13 (c) illustrates our result. The visualizations indicate that, due to the global receptive field provided by the proxy, our method achieves more consistent and dependable segmentation results overall, thus enhancing segmentation performance.

Failed Cases. Fig. 14 illustrates the failed cases of our method on the Scannet dataset [10]. In Fig. 14, it is apparent that the proxy is failed to address the classification error attributed to location fusion. Consequently, achieving a proper balance between local and global information still requires further investigation.

A.4. Open Source.

The supplementary material includes the training and testing code along with the configuration files. In addition, we have shared a link to an anonymous GitHub repository which contains the training logs and the val / test result for our model. Furthermore, we provide test results for other models including Swin3d [45], OctFormer [40], and PTv3 [44] in

Indoor Semantic		Indoor Instance	
Config	Value	Config	Value
framework	/	frame	PointGroup
optimizer	AdamW	optimizer	AdamW
scheduler	Cosine	scheduler	Cosine
criteria	CrossEntropy (1) Lovasz [2] (1)	criteria	/
weight decay	5e-2	weight decay	5e-2
batch size	12	batch size	12
datasets	ScanNet / S3DIS	datasets	ScanNet
First Stage:			
learning rate	5e-3	learning rate	5e-3
block lr scaler	0.1	block lr scaler	0.1
warmup epochs	40	warmup iters	40
epochs	800	epochs	800
Second Stage:			
learning rate	2e-4	learning rate	2e-4
block lr scaler	1.0	block lr scaler	1.0
warmup epochs	20	warmup iters	20
epochs	400	epochs	400

Table 11. Indoor semantic / instance segmentation settings.

Outdoor Semantic			
Config	Value	Config	Value
optimizer	AdamW	datasets	NuScenes
scheduler	Cosine	weight decay	5e-3
criteria	CrossEntropy (1) Lovasz [2] (1)	batch size	12
		datasets	NuScenes
First Stage:			
learning rate	2e-3	epochs	50
block lr scaler	1e-1	warmup epochs	2
Second Stage:			
learning rate	2e-4	epochs	30
block lr scaler	1.0	warmup epochs	1

Table 12. Outdoor semantic segmentation settings.

the repository for both Scannet and Scannet200 for peer review. We will release the weight of our model if the paper is accepted.

B. Implementation Details

Our implementation primarily utilizes Pointcept [9], a specialized codebase focusing on point cloud perception and representation learning. The details of our implementation are detailed in this section.

B.1. Training Settings

Datasets and metrics. The ScanNet dataset [10, 32], frequently utilized in indoor real-world down-stream tasks, contains 1,513 room scans derived from RGB-D frames, with 1,201 scenes designated for training and 312 reserved for validation. Each point was categorized into one of the 20

Config	Indoor	Outdoor
Proxy embedding depth		2
Proxy embedding temperature	10	1
Proxy init method		Spatial-wise
Proxy number	160	400
Proxy search range	[0.0, 1.0]	[0.0, 20.0]
Proxy search iter	10	16
Association method		Vertex-based
Association dim	3	2
Attention channels per head		16
Attention dropout		0.0
TRB table size		16
TRB table strength		1.0
TRB table temperature		[0.5, 2.5]
Point-Proxy TRB input scale	2.5	0.2
Proxy-wise TRB input scale	0.4	0.04
Drop path		0.3

Table 13. Model settings.

Augmentations	Parameters	Indoor	Outdoor
random dropout	dropout ratio: 0.2, p: 0.2	✓	-
random rotate	axis: z, angle: [-1, 1], p: 0.5	✓	✓
	axis: x, angle: [-1 / 64, 1 / 64], p: 0.5	✓	-
	axis: y, angle: [-1 / 64, 1 / 64], p: 0.5	✓	-
random scale	scale: [0.9, 1.1]	✓	✓
random flip	p: 0.5	✓	✓
random jitter	sigma: 0.005, clip: 0.02	✓	✓
elastic distort	params: [[0.2, 0.4], [0.8, 1.6]]	✓	-
auto contrast	p: 0.2	✓	-
color jitter	std: 0.05; p: 0.95	✓	-
grid sampling	grid size: 0.02 (indoor), 0.05 (outdoor)	✓	✓
sphere crop	ratio: 0.8, max points: 128000	✓	-
normalize color	p: 1	✓	-

Table 14. Data augmentations.

semantic labels in ScanNet [10] and 200 semantic labels in ScanNet200 [32]. In contrast, the S3DIS dataset [1] covers 271 rooms in six areas within three buildings with 13 categories. nuScenes [3] consists of 40,157 annotated samples, each containing six monocular camera images that cover a 360-degree field of view and a 32-beam LiDAR. According to the specifications of nuScenes, the dataset is composed of 1000 scenarios, 1.4M images, and 400K point clouds. The training set covers 700 scenarios, and both the validation and test sets contain 150 scenarios each. For metrics, we utilize the mean class-wise intersection over union (mIoU) as the principal metric in ScanNet, ScanNet200, and S3DIS. Furthermore, following previous work, area 5 in S3DIS is designated for testing with a 6-fold cross-validation.

Indoor semantic segmentation. The setting for indoor semantic segmentation is displayed in Tab. 11. The SP²T model was trained in two phases. In the first stage, emphasis is placed on local fusion, using the local fusion network for separate training on Scannet [10] or S3DIS [1]. Hence, the model incorporates the weights of local fusion into the

second training phase.

Indoor instance segmentation. Followed by PTV3 [44], we use PointGroup [19] as our foundational framework. Specifically, our configuration mainly follows PTV3. In addition, as with semantic segmentation, the model was trained in two stages.

Outdoor semantic segmentation. Similarly to indoor segmentation, Tab. 12 outlines the training parameters for SP²T when applied to outdoor segmentation. Similarly to our approach for indoor segmentation, the model undergoes a two-stage training process. Initially, in the first stage, a distinct local fusion network is trained specifically for nuScenes. Then, for the second stage, the model is initialized with the parameters of this local fusion network and continues to train.

B.2. Model Settings

Tab. 13 presents a comprehensive overview of our model’s configuration, focusing primarily on the proxy’s initialization and association method, table-based relative bias and dropout [35]. Furthermore, the parameters for local fusion mirror those of the specific methods [7, 44], and the proxy channel is the same as the channel of local fusion.

B.3. Data Augmentations

As illustrated in Tab. 14, we adopted the PTV3 [44] data augmentation approach to maintain fairness during both training and evaluation. In addition, we applied the same data enhancement to the test set and evaluated other models using this augmentation.